J. Fluid Mech. (2011), *vol.* 668, *pp.* 223–235.
doi:10.1017/S0022112010005690

Dynamics of inertial particles in a turbulent von Kármán flow

R. VOLK†, E. CALZAVARINI, E. LÉVÊQUE AND J.-F. PINTON

International Collaboration for Turbulence Research, Laboratoire de Physique de l'École Normale Supérieure de Lyon, UMR5672, CNRS et Université de Lyon, 46 Allée d'Italie, 69007 Lyon, France

(Received 27 January 2010; revised 27 October 2010; accepted 27 October 2010)

We study the dynamics of neutrally buoyant particles with diameters varying in the range [1, 45] in Kolmogorov scale units (η) and Reynolds numbers based on Taylor scale (Re_λ) between 590 and 1050. One component of the particle velocity is measured using an extended laser Doppler velocimetry at the centre of a von Kármán flow, and acceleration is derived by differentiation. We find that the particle acceleration variance decreases with increasing diameter with scaling close to $(D/\eta)^{-2/3}$, in agreement with previous observations, and with a hint for an intermittent correction as suggested by arguments based on scaling of pressure spatial increments. The characteristic time of acceleration autocorrelation increases more strongly than previously reported in other experiments, and possibly varying linearly with D/η. Further analysis shows that the probability density functions of the acceleration have smaller wings for larger particles; their flatness decreases as well, as expected from the behaviour of pressure increments in turbulence when intermittency corrections are taken into account. We contrast our measurements with previous observations in wind-tunnel turbulent flows and numerical simulations.

Key words: homogeneous turbulence, isotropic turbulence, particle/fluid flows

1. Introduction

Research in dynamics and transport phenomena in turbulence has recently benefited from experimental tracking of flow tracers (see for instance Ott & Mann 2000; La Porta *et al.* 2001; Mordant *et al.* 2001; Arneodo *et al.* 2008; Toschi & Bodenschatz 2009). Ideally, these tracers should have a size much smaller than the Kolmogorov length (η) at which the velocity gradients are smooth and hence their motion follows fluid streamlines, but experimental constraints have often led to the use of larger particles – with some bias as discussed e.g. by Mei (1996) and Brown, Warhaft & Voth (2009). On the other hand, the question of the dynamics of objects with a finite size freely advected by turbulent motions remains. Indeed, while theories developed in the small particle limit and vanishing particle Reynolds numbers Re_p yield the widely used Maxey–Riley–Gatignol equation, the equation of motion of a large particle with high-Re_p is largely unknown (see, however, Auton, Hunt & Prud'homme 1988; Lovalenti & Brady 1993; Loth & Dorgan 2009). A recent systematic analysis has been made in a wind tunnel ($Re_\lambda = 160$) using helium-inflated soap bubbles (Qureshi

† Email address for correspondence: romain.volk@ens-lyon.fr

et al. 2007, 2008). Other studies were performed with neutrally buoyant polystyrene particles in water in a turbulent von Kármán (VK) flow ($Re_\lambda \in [400, 815]$)(Voth *et al.* 2002; Brown *et al.* 2009). These studies have obtained several noteworthy results. (i) The variance of acceleration decreases as $D^{-2/3}$, consistent with the scaling of pressure increments in Kolmogorov's phenomenology of turbulence. The influence of varying Reynolds numbers ($Re_\lambda \in [400, 815]$) has also been studied in Brown *et al.* (2009), showing that the variance of acceleration actually scales according to $\epsilon^{3/2}\nu^{-1/2}(D/\eta)^{-2/3}$. (ii) The probability distribution functions (PDFs) of acceleration components do not depend on particle sizes in the range explored, $D/\eta \in [12, 25]$ (Qureshi *et al.* 2007) and $D/\eta \in [0.4, 27]$ (Brown *et al.* 2009). Brown *et al.* (2009) note that PDFs for large particle sizes may have slightly reduced wings as compared to the fluid particle PDF. However, because of systematic uncertainties, they do not draw any firm conclusion. A numerical study based on the Faxén model (Calzavarini *et al.* 2009) suggests that the PDF flatness should decrease with increasing particle size for $Re_\lambda = 75, 180$. This finding is questioned by a more recent numerical study (Homann & Bec 2010) based on a direct simulation approach using penalty methods, which finds a collapse of the PDFs for $D/\eta \in [2, 14]$ at $Re_\lambda = 32$. Following these studies, we have collected new experimental data using an extended laser Doppler velocimetry (LDV) technique in a VK flow (improved experiment from Volk *et al.* 2008*b*). We observe as follows. (i) There may be intermittent corrections to the $(D/\eta)^{-2/3}$ scaling of acceleration variance. (ii) The acceleration PDFs normalized by their variance are not independent of the particle size. Our statistical analysis shows that the wings of the distributions become less extended as D/η increases. (iii) The response time of the particle, as computed from the acceleration autocorrelation function, increases more strongly than that computed from wind-tunnel or DNS data (reported by Calzavarini *et al.* 2009), and possibly linearly with D/η.

2. Description of the experiment

2.1. *Experimental set-up*

The flow is of the von Kármán type and uses the same set-up as described by Volk *et al.* (2008*a*). Water fills a cylindrical container of internal diameter 15 cm, height $H = 25$ cm. It is driven by two counter-rotating disks of diameter $2R = 14$ cm, fitted with eight straight blades of height 0.5 cm in order to impose inertial steering (figure 1*a*). The distance between the disks is 20 cm and the rotation rate Ω is fixed at values up to 10 Hz, with two calibrated DC motors driven with a constant voltage. The angular velocity of the disks, directly measured from the tachometers of the motors, is adjusted so that they rotate at the same velocity but in opposite directions. Their rotation rate remains constant in time with a precision of about 2 %. This inertial forcing generates a fully turbulent flow ($Re_\lambda > 400$) in a compact region of space. This is why the von Kármán counter-rotating flow has been used in many studies of very-high-Reynolds-number turbulence, both for studies focusing on Eulerian quantities (see, for example, Zocchi *et al.* 1994) and on Lagrangian statistics (La Porta *et al.* 2001; Mordant *et al.* 2001; Voth *et al.* 2002). As opposed to wind-tunnel (WT) flows, the von Kármán flow has a mean three-dimensional spatial structure (figure 1*b*). As the disks rotate in opposite directions, the flow has a large azimutal component with a strong gradient in the axial (z) direction. It is of the order of $2\pi R\Omega$ close to the disks, and zero in the midplane ($z = 0$) of the cylinder. Because we use blades to improve stirring, the disks also act as centrifugal pumps ejecting the fluid radially at the top and bottom of the set-up, resulting in a large scale poloidal

Ω (Hz)	u_{rms} (m s^{-1})	a_{rms} (m s^{-2})	τ_η (ms)	η (μm)	ϵ (W kg^{-1})	Re_λ (–)	a_0 (–)
4.1	0.57	144	0.53	24.8	4	590	2.8
6.4	0.85	375	0.33	19.6	10.2	815	4.6
7.2	0.99	496	0.28	18.2	13.9	950	5.1
8.5	1.17	706	0.19	16.2	21.8	1050	5.2

TABLE 1. Parameters of the flow. Ω, rotation rate of the disks; ϵ, dissipation rate, from the power consumption of the motors. Note that u_{rms} and a_{rms} are computed using the x-component of the velocity, and the Taylor-based Reynolds number is estimated as $Re_\lambda = \sqrt{15u_{rms}^4/\epsilon\nu}$. a_0 is derived from the Heisenberg–Yaglom relation $a_0 \equiv a_{rms}^2 \nu^{1/2}\epsilon^{-3/2}$.

recirculation with a stagnation point in the geometrical centre of the cylinder. The flow proved to be locally homogeneous in the central region (Marié & Daviaud 2004), but non-isotropic at both large and small scales (Voth *et al.* 2002), the small scales approaching isotropy in the very-high-Re_λ limit.

The dissipation rate ϵ is computed from the global power consumption of the flow with the formula $\epsilon = 2(P_{water} - RI_{water}^2 - P_{air} + RI_{air}^2)/M$, where P is the power consumption of one motor, R is the electrical resistance of the rotor, I is the electrical current, M is the total mass of fluid, and the indices denote measurements with water or air filling the vessel. This procedure removes the Joule and mechanical friction contributions and yields an estimation of ϵ in agreement with Zocchi *et al.* (1994), who have measured the local dissipation ϵ from hot-wire anemometry in flows with the same geometry. For the measurements reported here, the flow temperature is regulated at 15° C for all rotation rates. The Taylor-based Reynolds number, computed with the formula $Re_\lambda = \sqrt{15u_{rms}^4/\epsilon\nu}$ using the x-component of the velocity to scale the velocity fluctuations, ranges from 590 to 1050, with a maximum dissipation rate ϵ equal to 22 W kg^{-1} (table 1). The Eulerian measurement of pressure has been performed with a Kistler 7031 pressure sensor mounted flush with the lateral wall, in the midplane of the experiment (figure 1).

2.2. *Extended laser Doppler velocimetry*

The particles, which are tracked in a small volume located in the geometrical centre of the cylinder, have a density of 1.06, with diameters $D = 30, 150, 250, 430, 750$ μm. Further changing the flow stirring will correspond to $D/\eta \in [1, 45]$. In order to measure the velocity of the particles along their trajectories, we use the extended laser Doppler velocimetry (eLDV) introduced by Volk *et al.* (2008*a*,*b*). We use wide laser beams intersecting in the centre of the flow to illuminate particles on a significant fraction of their path (figure 1*c*). In the set-up, the axis of rotation is vertical and the laser beams are horizontal, resulting in fringes perpendicular to the x-axis. When a particle crosses the fringes, the scattered light is then modulated at a frequency directly proportional to the x-component of the velocity (denoted u_x). As the beams are not collimated, the inter-fringe remains constant across the measurement volume, whose size is about $5 \times 5 \times 10\,\text{mm}^3$. In practice, we use a 2W continuous Argon laser of wavelength 514 nm, with single longitudinal mode and stabilized power output, to impose a 41 μm inter-fringe. The measurement volume is imaged on a low noise Hamamatsu photomultiplier in the case of the smallest (fluorescent) particles, while for larger particles, the detection is made using a PDA-36A photodiode from Thorlab. In order to get the sign of the velocity, we use two acousto-optic modulators (AOM)

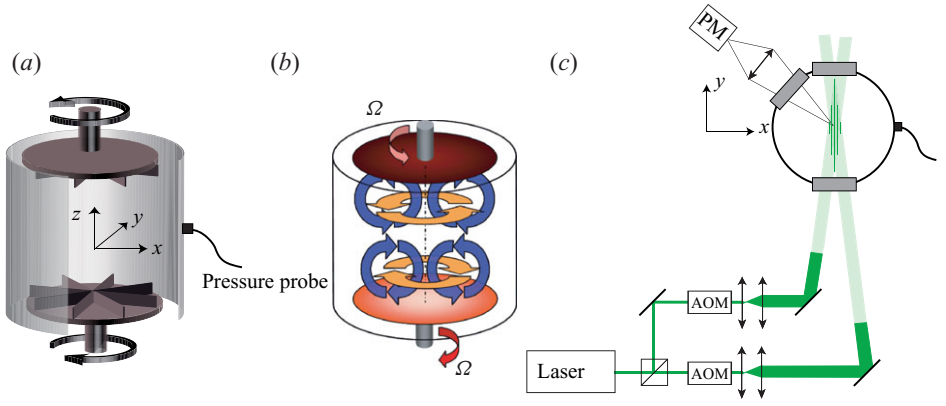

FIGURE 1. (Colour online) Experimental set-up. (*a*) Geometry of the turbulence generator. (*b*) Schematics of the von Kármán flow in water. (*c*) Principle of the LDV using wide beams (eLDV) – top view of the experiment. PM denotes location of the photomultiplier which detects scattering light modulation as a particle crosses the interference pattern created at the intersection of the laser beams. The eLDV measures, for one particle at a time, the evolution of its velocity component $u_x(t)$ along the particle trajectory.

to impose a 100 kHz frequency shift between the beams so that the fringes are actually travelling at a constant speed. The output is recorded using a National Instrument PXI-NI5621 16-bit digitizer at rate 1 MHz. The velocity is computed from the light-scattering signal using a demodulation algorithm described by Mordant, Michel & Pinton (2002), with a time resolution adjustable in the range [5–30] μs. We adjust the seeding density to be low enough so that we do not observe events with two particles at the same time in the measurement volume, but high enough to observe at least one trajectory per second. The output of the measurement is a collection of 15 000 trajectories $(u_x^n(t))_n$ of mean duration of 20 Kolmogorov times (τ_η), from which the acceleration $(a_x^n(t))_n$ is computed by differentiation. Because of measurement noise, the signal has to be filtered using a Gaussian smoothing kernel with window width w as proposed by Mordant, Crawford & Bodenschatz (2004*a*). Moments of the statistics of fluctuations of acceleration are computed for varying values of w and extrapolated to zero filter width as in Volk *et al.* (2008*a*). Note that the argon laser used in this study is stabilized both in power output and phase (with single longitudinal mode in the cavity). This improvement leads to a better estimation of the acceleration variance; therefore, the values of a_0 reported in table 1 are 20 % smaller than those in Volk *et al.* (2008*a*).

3. Results

3.1. *Particle velocitiy*

One expects that Eulerian and Lagrangian velocity statistics coincide under ergodicity approximation, so that the tracer-particle velocities are expected to have Gaussian statistics. Our observation is that the velocity distribution is markedly sub-Gaussian as seen in figure 2(*a*) – flatness values are (2.56, 2.58, 2.62, 2.46) for the four Reynolds number values explored in this work. Sub-Gaussian statistics for the velocity have been observed in many experimental set-ups, however usually less pronounced than in our case. Flatness values for velocities in WT flow are closer to three (M. Bourgoin

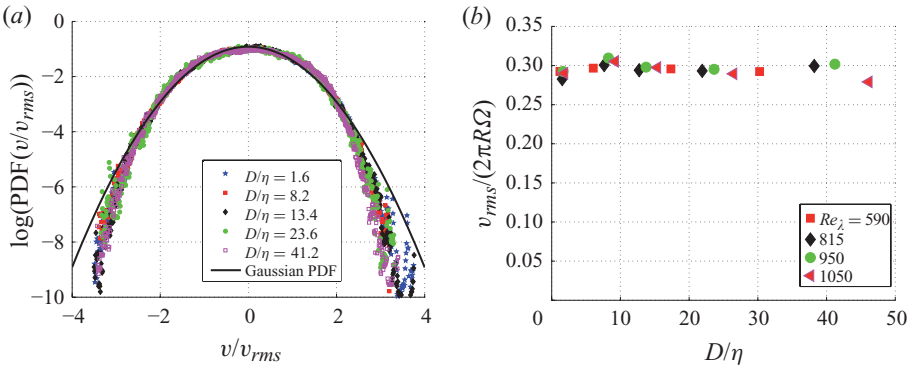

FIGURE 2. (Colour online) (*a*) PDF of particle velocities. (*b*) Evolution of the r.m.s. velocity of the particles normalized by the disk velocity $2\pi R\Omega$ as a function of particle size for the different Reynolds numbers studied.

private communication). Here the VK flow has a large-scale inhomogeneity and anistropy (cf. Voth *et al.* 2002; Marié & Daviaud 2004; Volk, Odier & Pinton 2006), which may enhance the sub-Gaussianity. In such a confined geometry, the VK flow is known to have several possible configurations of its large-scale velocity profile (Monchaux *et al.* 2006; de la Torre & Burguete 2007); each configuration may lead to Gaussian velocity fluctuations about a locally different mean value with an overall effect leading to a sub-Gaussian histogram. However, we have not observed any change in the velocity statistics when the Reynolds number is increased or when the size of the particle is changed by over an order of magnitude in D/η. In fact, for this fully turbulent regime, the velocity variance is equal to 30 % of the impeller tip speed, as can be seen in figure 2(*b*). As shown by Ravelet, Chiffaudel & Daviaud (2008), this is a characteristic of the von Kármán driving impellers, and not a characteristic of the inertial particle size. We note that this observation is in agreement with a prediction following Faxén argument at the leading order, $v^2/u^2_{fluid} = 1-(5/12)(D^2/\lambda^2)$ (Homann & Bec 2010) – where λ is Taylor's microscale, giving a correction smaller than 1 % for the Taylor-based-Reynolds-number range considered here.

3.2. *Particle acceleration variance*

With one component of velocity probed by the eLDV system and in a situation in which the direction of motion is not prescribed, the first moment of the distribution of acceleration is zero. One expects that the second moment (acceleration variance) reduces with increasing particle size, because the pressure forces which mainly cause the motion are averaged over a growing area. As shown in figure 3, this is indeed observed. The evolution of the acceleration variance measured here is in qualitative agreement with previous studies by Voth *et al.* (2002), Qureshi *et al.* (2007) and Brown *et al.* (2009): when normalized by the acceleration variance of the smallest particles (fluid tracers, denoted as $\langle a_T^2\rangle$), the quantity $\langle a_D^2\rangle/\langle a_T^2\rangle$ exhibits a decrease consistent with the power-law $(D/\eta)^{-2/3}$ for all Reynolds numbers and inertial range particle sizes. Recall that this power-law behaviour is obtained when one assumes that the particle acceleration scales like pressure increments over a length proportional to the particle's diameter. In the inertial range of scales, this argument yields the scaling $\langle a_D^2\rangle \propto \langle(\delta_D P/D)^2\rangle \sim D^{4/3-2} = D^{-2/3}$, where $\langle(\delta_D P)^n\rangle \equiv S_p^n(D)$ is the pressure nth-order spatial structure function. Later, we show that one may also include

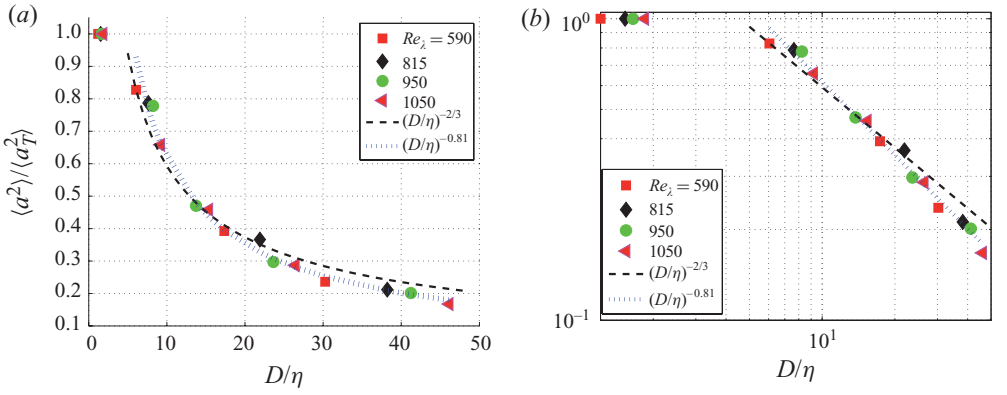

FIGURE 3. (Colour online) (*a*) Variance of one component of acceleration of the particles versus particle size. (*b*) The same figure in log-log representation. In order to be able to compare flows at varying Reynolds numbers Re_λ, the particle acceleration variance is normalized by the one measured with the smallest particles (tracers (T), for which $D/\eta \leqslant 2$ at all Re_λ), and diameters are normalized by the viscous dissipative scale η. Thick solid line denotes Kolmogorov scaling $\langle a_D^2 \rangle \propto (D/\eta)^{-2/3}$. Thin dashed line denotes refinement including intermittency corrections (see details in § 3.4).

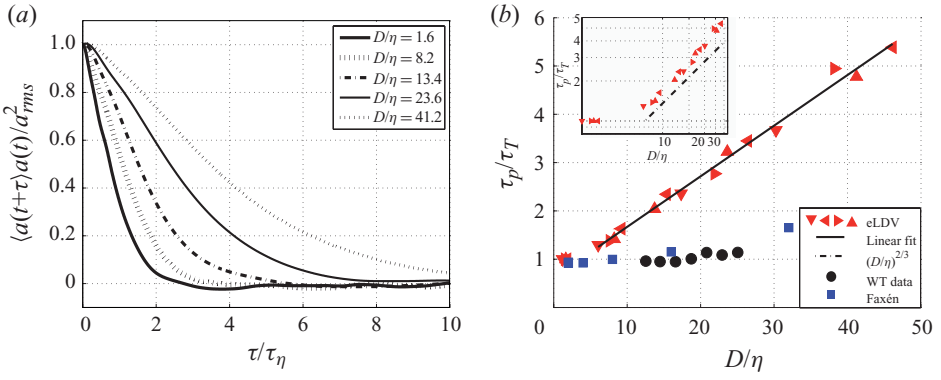

FIGURE 4. (Colour online) (*a*) Particle acceleration autocorrelation functions for $Re_\lambda = 950$; (*b*) evolution of particle response times. The wind-tunnel and Faxén data are extracted from Calzavarini *et al.* (2009) ($Re_\lambda = 160$ for wind-tunnel data and $Re_\lambda = 180$ for Faxén model data). For the eLDV data, the symbols correspond to increasing Reynolds numbers: ▼, $Re_\lambda = 590$; ◀, $Re_\lambda = 815$; ▶, $Re_\lambda = 850$; ▲, $Re_\lambda = 1050$. (inset) Log–log of the particle response times (triangles) together with a $(D/\eta)^{2/3}$ power law (dashed line).

intermittency corrections to obtain the dashed line in figure 3, which yields an improved fit of our experimental data.

3.3. *Particle response time*

A characteristic time for the evolution of a particle response to flow changes is obtained from the acceleration autocorrelation functions. Their shape and evolution with particle size are shown in figure 4(*a*), for $Re_\lambda = 950$. In agreement with previous observations for tracers, the autocorrelation for small particles vanishes in times of the order of a few Kolmogorov times $\tau_\eta = \sqrt{\nu/\epsilon}$. As expected, the response time τ_p, defined as the integral over time of the positive part of $C_{aa}(\tau)$, increases with size, at

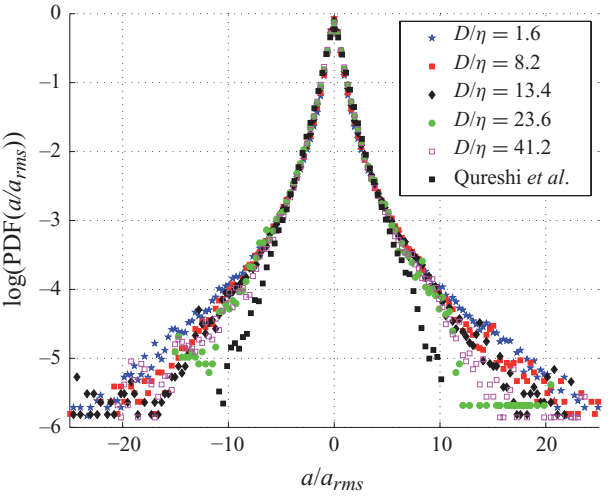

FIGURE 5. (Colour online) PDFs of particle acceleration at $Re_\lambda = 950$, normalized by their variance. The wind-tunnel data of Qureshi *et al.* (2007, 2008) correspond to $Re_\lambda = 160$.

any given Reynolds number. Our observation is that for a given Reynolds number, τ_p increases *linearly* with the particle diameter D for sizes larger than about 10η. In addition, as shown in figure 4(*b*)(red/triangle symbols), measurements performed at various Re_λ all line-up on the same curve when τ_p is normalized by the response time of the smallest particles (tracers, T) for which $\tau_T = (1.07 \pm 0.16)\tau_\eta$. This confirms that the evolution is indeed given by the relevant dimensionless variables, $\tau_p/\tau_\eta = f(D/\eta)$, i.e. when the response time is counted in units of the Kolmogorov time $\tau_\eta = \sqrt{\nu/\epsilon}$ and the particle size is counted in units of the dissipative scale $\eta = (\nu^3/\epsilon)^{1/4}$.

The behaviour observed is quite different from the prediction of point-particle (PP) models, for which the Stokes drag term becomes rapidly negligible when the particle size increases, so that the response time remains that of fluid tracers (Volk *et al.* 2008*a*). A first refinement of the PP model is to account for size effects by averaging the flow fields over the area of the particle (for the estimation of drag) and over its volume (for added mass effects); this is the essence of the Faxén-corrected model introduced by Calzavarini *et al.* (2009). Using this model, the authors have observed a variation of the particle response time with size: it increases by almost a factor of 2 when the size of the particle increases from $D = 2\eta$ to up to $D = 32\eta$. This finding was in general agreement with experimental measurement in a wind tunnel by Qureshi *et al.* (2008). As shown in figure 4(*a*), our measurements in a von Kármán flow show a much steeper increase: the response time of the particles is about four times that of the tracers when the diameter has grown to 32η, and the variation is roughly linear when plotted in linear coordinates. However, as shown in figure 4(*b*), the scaling $\tau_p/\tau_\eta = (D/\eta)^{2/3}$ cannot be excluded; it is obtained by assuming that the response time of the particle scales as the eddy turnover time of flow motions at a scale equal to the particle diameter.

3.4. *Particle acceleration probability density function*

The estimation of higher even moments of particle accelerations requires specific data processing, as we show in the following. We first discuss the raw distributions of the accelerations. In figure 5, they are shown for $Re_\lambda = 950$; the particle accelerations have been normalized by their variance (whose behaviour has been discussed in § 3.2).

To leading order, the distribution functions are very similar, as observed in the wind-tunnel measurements by Qureshi *et al.* (2007, 2008). There is no reduction to Gaussian statistics as the particle size grows well into the inertial range (see also Gasteuil 2009 for measurements with particles with integral range sizes). In figure 5, the PDF for the smallest particles is identical to that measured for tracers by Voth *et al.* (2002) in another VK flow, and in numerical simulations by Yeung (2002) and Mordant, Lévêque & Pinton (2004*b*). It is different from the PDFs reported by Qureshi *et al.* (2007, 2008) from wind-tunnel measurements at $Re_\lambda = 160$. These differences are more pronounced than what could be expected from Reynolds-number variations alone between the experiments. The first explanation could be that the acceleration PDFs are not universal but flow-dependent. This hypothesis is supported by the results of Voth *et al.* (2002), who showed that the Lagrangian small-scale dynamics still reflects the anisotropy of the large scales. The second possibility is that the acceleration PDFs measured by Qureshi *et al.* are not the PDFs one would measure for tracers in a WT flow. This explanation is supported by the work of Ayyalasomayajula, Warhaft & Collins (2008), who showed that water droplets (which behave as tracers in wind-tunnel turbulence at $Re_\lambda = 180$) have an acceleration PDF with more extended tails than those reported by Qureshi *et al.* (2007). This would mean that the acceleration PDFs of material particles do change significantly with increasing size.

Investigating the possibility of changes in the statistics of acceleration with size or Reynolds number can be done by studying higher-order moments, starting with the distribution flatness. It requires a converged measurement of the PDFs and, as shown for tracer particles by Mordant *et al.* (2004*a*), this implies extremely large data sets. As a first attempt, we fit the acceleration PDF with a model functional form which we then use to *estimate* the flatness of the distribution. The procedure is as follows. We assume that the statistics is described by a functional form $\mathscr{F}_\theta(x = a/a_{rms})$; $\{\theta\}$ is a set of adjustable parameters which are determined by minimizing the distance $x^2\mathrm{PDF}(x) - x^2\mathscr{F}_\theta(x)$, where $\mathrm{PDF}(x)$ is the measured distribution. Two trial distributions have been tested:

$$\mathscr{F}_s^{LN}(x) = \frac{\mathrm{e}^{3s^2/2}}{4\sqrt{3}}\left(1 - \mathrm{erf}\left(\frac{\ln|x/\sqrt{3}| + 2s^2}{s\sqrt{2}}\right)\right), \tag{3.1}$$

which stems from the assumption that the acceleration amplitude has a lognormal distribution (s being the only adjustable parameter), and a stretched exponential functional form

$$\mathscr{F}_s^{SE}(x) = A\,\exp\left(\frac{-x^2}{2\sigma^2\left(1 + \left|\dfrac{x\beta}{\sigma}\right|^\gamma\right)}\right), \tag{3.2}$$

(A being a normalization constant) which has three adjustable parameters (σ, β, γ), and allows us for a finer adjustment of the distribution in the tails. Note that with distributions having such extended wings, a 'brute force' measurement of the flatness factor within a 5 % accuracy would mean a resolution of the distribution up to about 100 standard deviations, and events with probability below 10^{-11} – clearly outside of direct experimental reach.

Figure 6 shows a comparison of the acceleration PDF for the smallest particles at $Re_\lambda = 815$ and the corresponding fits that minimize the distance to the quantity $x^2\mathrm{PDF}(x)$ in the range $x = a/a_{rms} \in [-25, 25]$. As one can see, both functional forms fit correctly the experimental data up to $a/a_{rms} \sim 20$, the stretched exponential form

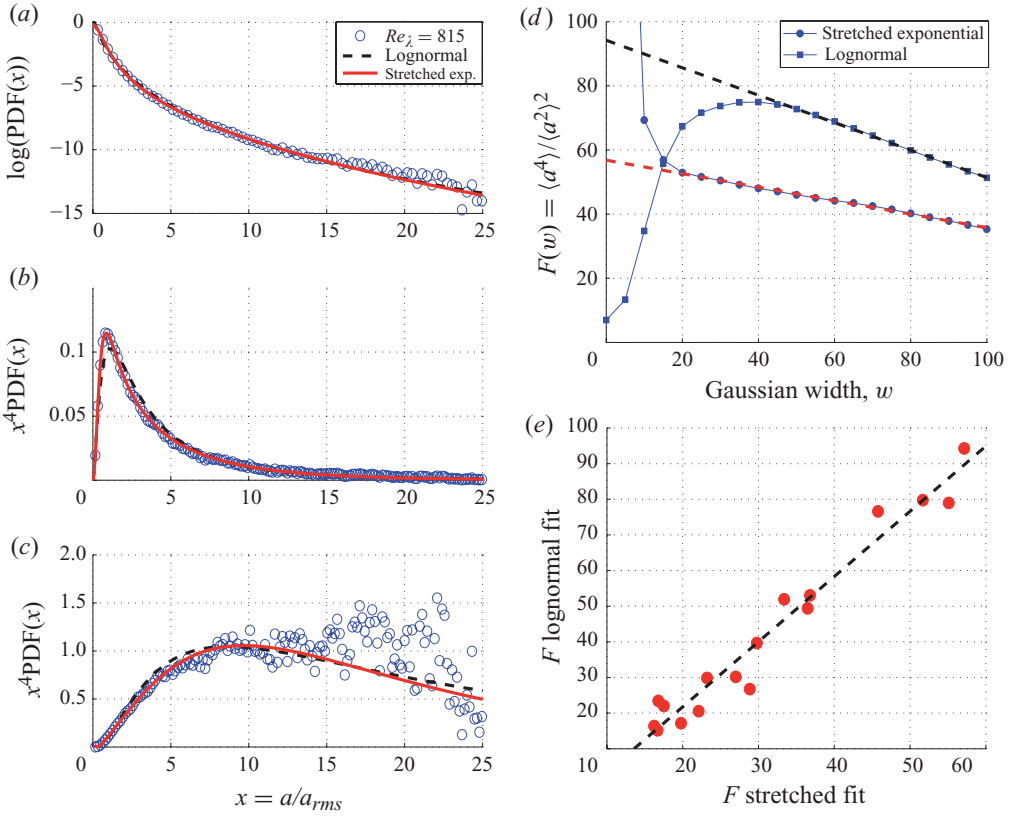

FIGURE 6. (Colour online) (*a*): PDF of particle acceleration with $D/\eta = 1.5$ at $Re_\lambda = 815$ and the corresponding lognormal (dashed line) and stretched exponential (exp., solid line) fits. The data have been processed using a Gaussian smoothing with width $w = 20$. (*b*) Linear plot of the second-order moment $x^2\mathrm{PDF}(x)$ with corresponding fits. (*c*) Linear plot of $x^4\mathrm{PDF}(x)$ with the lognormal and stretched exponential fits. (*d*) Evolution of the flatness $F(w) = \langle a^4\rangle/\langle a^2\rangle^2$ as a function of the width of the Gaussian window (w) for the lognormal estimator (■) and the stretched exponential estimator (●). For both curves, the dashed line is the linear fit of $F(w)$ in the region $w \in [50, 100]$, leading to an extrapolated flatness $F_L = 94$ for the lognormal estimator and $F_S = 57$ for the stretched exponential estimator. (*e*) Relative evolution of the flatness F estimated with the two estimators. (●), experimental data; dashed line, linear fit $F_D = 1.83\,F_S - 14.8$.

showing a better agreement with the second-order moment. As reported in previous studies, the moments of the acceleration PDFs strongly depend on the width w of the smoothing kernel used to extract the velocity data from the modulated optical signal (cf. § 2). We thus estimate the flatness by fitting the different PDFs for decreasing w and then by interpolating to zero width. The result of this procedure is shown in figure 6(*d*) for the two trial functional forms. As can be seen, the flatness derived from the lognormal estimator is roughly 1.6 higher than that computed from the stretched exponential estimator. As the two trial distributions model the wings of the PDFs in a different way, we find that the flatness estimated from the two functions is not strictly proportional to each other, but is related by a linear relationship as shown in figure 6(*e*). The values of the flatness reported have to be taken as estimates, the true values strongly depending on the real shape of the acceleration PDF in the far tails.

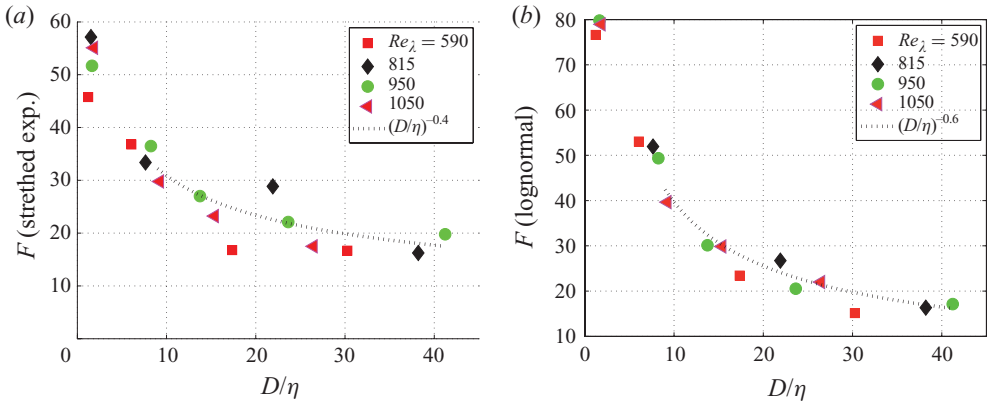

FIGURE 7. (Colour online) Variation of the estimated flatness as a function of D/η for different sizes and different Reynolds numbers. (a) Stretched exponential (exp.) estimator and (b) lognormal estimator.

We propose however that the *variations* detected here yield a first-order estimation of the evolution of acceleration statistics with particle size.

The results are shown in figure 7(a,b). For both estimators, one observes a reduction in the flatness with increasing particle sizes. This can be understood if one takes into account the intermittency of the pressure increments for inertial range separations. Following the approach developed by Voth *et al.* (2002), Qureshi *et al.* (2007) and Brown *et al.* (2009), one estimates the acceleration flatness $F(D)$ by assuming that the force acting on the particles is dominated by the pressure gradient over a length scale proportional to D. All moments of the acceleration ($\langle a_D^n \rangle$) should then scale as $S_P^n(D)/D^n$, with a behaviour dictated by pressure structure functions. Now, in order to estimate the pressure structure functions, one can either use the ansatz that pressure increments scale as the square of velocity increments, $\langle \delta_D P \rangle \propto \langle (\delta_D v)^2 \rangle$, or one can measure directly the scaling of pressure in the experiment. In the first case, one obtains $S_P^n(D) \propto D^{2\zeta_n}$, ζ_n being the structure function exponents of the Eulerian velocity increments. One then obtains $F(D) \propto D^{\zeta_8 - 2\zeta_4} \sim D^{-0.42}$, if one assumes a lognormal scaling for the Eulerian velocity structure functions as in Chevillard *et al.* (2006), independent of the Reynolds number.

In order to have an experimental measurement of pressure structure functions, we have recorded the pressure using a transducer mounted flush in the lateral wall, in the midplane of the flow. This measurement, although not performed in the bulk of the flow, yields $S_P^2 \propto D^{1.2 \pm 0.1}$ and $S_P^4/(S_P^2)^2 \propto D^{-0.38 \pm 0.03}$, power laws which are both in agreement with wind-tunnel data of Pearson & Antonia (2001) and Eulerian DNS data at $Re_\lambda = 180$ (from the same DNS described by Calzavarini *et al.* 2009). In the case of the stretched exponential estimator, these predictions for the scaling exponent are consistent with the value $\alpha \sim -0.4$ obtained by fitting the data with a power-law $F_s(D) = A(D/\eta)^\alpha$, with D/η in the range $[10, 40]$. In the case of the lognormal estimator, one finds a scaling law $F_l(D) \propto (D/\eta)^{-0.6}$. Here we stress that $\mathscr{F}_s^{LN}(a)$ and $\mathscr{F}_s^{SE}(a)$ are intrinsically different distributions; therefore, it is in principle impossible to fit both curves with the same scaling exponent. The true value of the exponent (if it exists) should depend on the real shape of the PDFs. However, the consistency between the estimation using the stretched exponential estimator and the Eulerian measurements of pressure suggests that this functional form is a good estimation of

the acceleration PDFs in the case of large acceleration flatness ($F > 20$). This was confirmed by comparing the quality of the two different estimators with numerical data obtained at $Re_\lambda = 180$ ($F \simeq 27.5$, Calzavarini *et al.* 2009). Using a truncated data set as a test, the stretched exponential estimator proved to yield a better fit than the lognormal estimator, and was able to give an estimate of the flatness only 15 % lower than the converged value computed using the whole data set.

Finally, we note that following the same approach, one can use the second-order pressure structure function to get a new estimation of the decrease of the acceleration variance $\langle a_D^2 \rangle$. Assuming a lognormal scaling for the velocity increments, one then finds $\langle a_D^2 \rangle \propto \langle (\delta_D P/D)^2 \rangle \sim D^{\zeta_4 - 2} = D^{-0.78 \pm 0.02}$ very close to the experimental measurements, which yields $\langle a_D^2 \rangle \sim D^{-0.8 \pm 0.1}$. These two values are in a very good agreement with the best fit shown by a dashed line in figure 3, which yields $\langle a_D^2 \rangle / \langle a_T^2 \rangle \propto (D/\eta)^{-0.81}$. In our opinion, this is an indirect proof that intermittency plays a role and that our results concerning the acceleration flatness, although preliminary, are consistent.

4. Concluding remarks

We have described here new eLDV measurements in an extended range of particle sizes. With an improved set-up and analysis techniques, we have obtained the evolution of the statistics of one component of the acceleration of the particles, and a measurement of a characteristic time of their response to flow changes. The response time is found to increase more steeply in our von Kármán flow than previously reported for wind-tunnel or DNS data. Concerning the statistics of acceleration fluctuations, we have investigated the behaviour of the second and fourth moments. The variance is well converged, and we have observed that in the study of its evolution with particle size, two normalization factors are important in order to collapse our observation on a single curve: the diameter should be scaled by the Kolmogorov dissipation length and the acceleration should be compared to that of tracer particles, which are more efficient at removing bias and Reynolds number effects than the Heisenberg–Yaglom scaling because $a_0 = \langle a^2 \rangle \epsilon^{-3/2} \nu^{1/2}$ is a function of Re_λ. The change of the flatness is *estimated* using model distributions. We have observed a steep evolution with particle size, particularly for $D < 10\eta$. Together with Reynolds number evolutions, this observation is consistent with the values reported for wind-tunnel turbulence (from $F \sim 25$–30, as measured for tracers by Ayyalasomayajula *et al.* 2008, to $F \sim 8$, as measured by Qureshi *et al.* 2007 for slightly larger particles). When looking for scaling properties of the variance or flatness of the acceleration, we have found that the variations are in agreement with the behaviour of pressure fluctuations; i.e. their evolution with scale is well predicted by the scaling of pressure increments over a separation proportional to the particle diameter. In fact, the best agreement between pressure increments and fluctuations of acceleration is obtained when intermittency corrections are added to mean field Kolmogorov arguments. Intermittency is natural in turbulence and well documented in VK flows. It may not be so surprising that it influences the statistics of motion of neutrally buoyant particles. Several points, however, deserve further studies in the future: the influence of the flow anisotropy must be quantified. To this end, we have recently devised a more symmetric version of VK flows driven by the rotation of 12 propellers, which has adjustable isotropy in the large scales (Zimmermann *et al.* 2010). Another point is the evolution when $D \sim L$, i.e. for particles approaching the integral scale. Power-law scaling may not be extended to this limit, and preliminary studies (Gasteuil 2009) in VK flows with comparable Reynolds numbers have

shown that the PDF of the accelerations of large particles ($D \sim L/5$) still has wide wings.

The authors thank Mickael Bourgoin for many useful discussions. This work was supported by grant ANR-BLAN-07-1-192604.

REFERENCES

Arneodo, A., Benzi, R., Berg, J., Biferale, L., Bodenschatz, E., Busse, A., Calzavarini, E., Castaing, B., Cencini, M., Chevillard, L., Fisher, R. T., Grauer, R., Homann, H., Lamb, D., Lanotte, A. S., Leveque, E., Luthi, B., Mann, J., Mordant, N., Muller, W. C., Ott, S., Ouellette, N. T., Pinton, J. F., Pope, S. B., Roux, S. G., Toschi, F., Xu, H. & Yeung, P. K. 2008 Universal intermittent properties of particle trajectories in highly turbulent flows. *Phys. Rev. Lett.* **100** (25), 254504-5.

Auton, T., Hunt, J. & Prud'homme, M. 1988 The force exerted on a body in inviscid unsteady non-uniform rotational flow. *J. Fluid Mech.* **197**, 241–257.

Ayyalasomayajula, S., Warhaft, Z. & Collins, L. R. 2008 Modeling inertial particle acceleration statistics in isotropic turbulence. *Phys. Fluids* **50**, 095104.

Brown, R., Warhaft, Z. & Voth, G. 2009 Acceleration statistics of neutrally buoyant spherical particles in intense turbulence. *Phys. Rev. Lett.* **103**, 194501.

Calzavarini, E., Volk, R., Lévêque, E., Bourgoin, B., Toschi, F. & Pinton, J.-F. 2009 Acceleration statistics of finite-size particles in turbulent flow: the role of Faxén corrections. *J. Fluid Mech.* **630**, 179–189.

Chevillard, L., Castaing, B., Lévêque, E. & Arneodo, A. 2006 Unified multifractal description of velocity increments statistics in turbulence: intermittency and skewness. *Physica* D **218**, 77–82.

Gasteuil, Y. 2009 Instrumentation Lagrangienne en turbulence: mise en oeuvre et analyse. PhD thesis, Ecole Normale Supérieure de Lyon.

Homann, H. & Bec, J. 2010 Finite-size effects in the dynamics of neutrally buoyant particles in turbulent flow. *J. Fluid Mech.* **651**, 81–91.

La Porta, A., Voth, G. A., Crawford, A. M., Alexander, J. & Bodenschatz, E. 2001 Fluid particle accelerations in fully developed turbulence. *Nature* **409**, 1017–1019.

Loth, E. & Dorgan, A. 2009 An equation of motion for particles of finite Reynolds number and size. *Environ. Fluid Mech.* **9**, 187–206.

Lovalenti, P. & Brady, J. 1993 The hydrodynamic force on a rigid particle undergoing arbitrary time-dependent motion at small Reynolds number. *J. Fluid Mech.* **256**, 561–605.

Marié, L. & Daviaud, F. 2004 Experimental measurement of the scale-by-scale momentum transport budget in a turbulent shear flow. *Phys. Fluids* **16**, 457–461.

Mei, R. 1996 Velocity fidelity of flow tracer particles. *Exp. Fluids* **22**, 1–13.

Monchaux, R., Ravelet, F., Dubrulle, B. & Daviaud, F. 2006 Properties of steady states in turbulent axisymmetric flows. *Phys. Rev. Lett.* **96**, 124502.

Mordant, N., Crawford, A. & Bodenschatz, E. 2004*a* Experimental Lagrangian acceleration probability density function measurement. *Physica* D **193**, 245–251.

Mordant, N., Lévêque, E. & Pinton, J. F. 2004*b* Experimental and numerical study of the Lagrangian dynamics of high Reynolds turbulence. *New J. Phys.* **6**, 116.

Mordant, N., Metz, P., Michel, O. & Pinton, J.-F. 2001 Measurement of Lagrangian velocity in fully developed turbulence. *Phys. Rev. Lett.* **87** (21), 214501.

Mordant, N., Michel, O. & Pinton, J.-F. 2002 Time-resolved tracking of a sound scatterer in a complex flow: non-stationary signal analysis and applications. *J. Acoust. Soc. Am.* **112**, 108–119.

Ott, S. & Mann, J. 2000 An experimental investigation of the relative diffusion of particle pairs in three-dimensional turbulent flow. *J. Fluid Mech.* **422**, 207–223.

Pearson, B. & Antonia, R. 2001 Reynolds-number dependence of turbulent velocity and pressure increments. *J. Fluid Mech.* **444**, 343–382.

Qureshi, N. M., Bourgoin, M., Baudet, C., Cartellier, A. & Gagne, Y. 2007 Turbulent transport of material particles: an experimental study of finite size effects. *Phys. Rev. Lett.* **99** (18), 184502.

Qureshi, N. M., Bourgoin, M., Baudet, C., Cartellier, A. & Gagne, Y. 2008 Turbulent transport of material particles: an experimental study of density effects. *Eur. Phys. J.* B **66**, 531–536.

Ravelet, F., Chiffaudel, A. & Daviaud, F. 2008 Supercritical transition to turbulence in an inertially driven von Kármán closed flow. *J. Fluid Mech.* **601**, 339–364.

de la Torre, A. & Burguete, J. 2007 Slow dynamics in a turbulent von Kármán swirling flow. *Phys. Rev. Lett.* **99**, 054101.

Toschi, F. & Bodenschatz, E. 2009 Lagrangian properties of particles in turbulence. *Annu. Rev. Fluid Mech.* **41**, 375–404.

Volk, R., Calzavarini, E., Verhille, G., Lohse, D., Mordant, N., Pinton, J. F. & Toschi, F. 2008*a* Acceleration of heavy and light particles in turbulence: comparison between experiments and direct numerical simulations. *Physica* D **237** (14–17), 2084–2089.

Volk, R., Mordant, N., Verhille, G. & Pinton, J. F. 2008*b* Laser Doppler measurement of inertial particle and bubble accelerations in turbulence. *Europhys. Lett.* **81** (3), 34002.

Volk, R., Odier, P. & Pinton, J.-F. 2006 Fluctuation of magnetic induction in von Kármán swirling flows. *Phys. Fluids* **18**, 085105.

Voth, G. A., La Porta, A., Crawford, A. M., Alexander, J. & Bodenschatz, E. 2002 Measurement of particle accelerations in fully developed turbulence. *J. Fluid Mech.* **469**, 121–160.

Yeung, P. K. 2002 Lagrangian investigations of turbulence. *Annu. Rev. Fluid Mech.* **34**, 115–142.

Zimmermann, R., Xu, H., Gasteuil, Y., Bourgoin, M., Volk, R., Pinton, J.-F. & Bodenschatz, E. 2010 The Lagrangian exploration module: an apparatus for the study of statistically homogeneous and isotropic turbulence. *Rev. Sci. Instrum.* **81** (5), 055112.

Zocchi, G., Tabeling, P., Maurer, J. & Willaime, H. 1994 Measurement of the scaling of dissipation at high Reynolds numbers. *Phys. Rev.* E **50** (5), 3693–3700.